Close-Stacking of Iron-Oxo-Based Double-Decker Complex on Graphite Surface Achieved High Catalytic CH_4 Oxidation Activity Comparable to that of Methane Monooxygenases

Yasuyuki Yamada,[1,2,3] Kentaro Morita,[1] Takuya Sugiura,[1] Yuka Toyoda,[1] Nozomi Mihara,[1] Masanari Nagasaka,[4] Hikaru Takaya,[4] Kiyohisa Tanaka,[4] Takanori Koitaya,[4] Naoki Nakatani,[5] Hiroko Ariga-Miwa,[6] Satoru Takakusagi,[6] Yutaka Hitomi,[3,7] Toshiji Kudo,[8] Yuta Tsuji,[9] Kazunari Yoshizawa,[9] and Kentaro Tanaka[1].

[1] Department of Chemistry, Graduate School of Science, Nagoya University, Furo-cho, Chikusa-ku, Nagoya 464-8602, Japan.
[2] Research Center for Materials Science, Nagoya University, Furo-cho, Chikusa-ku, Nagoya 464-8602, Japan.
[3] PRESTO/JST, 4-1-8 Honcho, Kawaguchi, Saitama 332-0012, Japan.
[4] Institute for Molecular Science, Myodaiji, Okazaki 444-8585, Japan.
[5] Department of Chemistry, Graduate School of Science, Tokyo Metropolitan University, 1-1 Minami-Osawa, Hachioji, Tokyo 192-0397, Japan.
[6] Institute for Catalysis, Hokkaido University, Kita 21-10, Kita-ku, Sapporo, Hokkaido, 001-0021, Japan.
[7] Department of Molecular Chemistry and Biochemistry, Graduate School of Science and Engineering, Doshisha University, Kyotanabe, Kyoto 610-0321, Japan.
[8] Daltonics Division, Bruker Japan K.K., 3-9, Moriya-cho, Kanagawa-ku, Yokohama-shi, Kanagawa, 221-0022, Japan.
[9] Institute for Materials Chemistry and Engineering and IRCCS, Kyushu University, 744 Motooka, Nishi-ku, Fukuoka 819-0385, Japan.

*E-mail: yamada.yasuyuki@h.mbox.nagoya-u.ac.jp, kentaro@chem.nagoya-u.ac.jp

Abstract

Inspired by the fact that methane monooxygenases (MMOs) utilize iron or copper oxo species as key intermediates, numerous biomimetic molecular catalysts have been developed. However, as methane is highly stable, there are no examples of biomimetic catalysts that show high catalytic activity, rivaling that of MMOs, in methane oxidation. Herein, we report that the close-stacking of a double-decker-type dinuclear iron phthalocyanine complex on a graphite surface is effective for achieving high methane oxidation activity, comparable to those of certain MMOs, in an aqueous solution. We propose that the stacking of the catalyst possibly induced partial charge transfer from the reactive oxo species of the double-decker complex and lowered the singly occupied molecular orbital (SOMO) level significantly, thereby facilitating proton-coupled electron transfer from methane. The decker structure is essential for the stable adhesion of the catalyst on the graphite surface, while maintaining its high oxo-basicity and oxo species generation rate. We also demonstrate that the graphite-supported catalyst exhibits significantly enhanced catalytic activity under photoirradiation because of the photothermal effect.

Introduction

Methane has long been predicted to be one of the next-generation feedstocks of the chemical industry because of its natural abundance in the natural gas, shale gas, or methane hydrate. It is also known that carbon dioxide can be converted into methane in the presence of hydrogen gas via the Sabatier reaction. However, methane produces a strong greenhouse effect. Therefore, both from the perspective of decreasing dependence on petroleum and from that of preventing global warming to meet the sustainable development goals, the demand for efficient catalysts that can catalyze the conversion of methane into more valuable raw chemicals has increased significantly.[1,2] However, efficient catalytic methane conversion at lower temperature has been well-recognized to be a formidable challenge in the field of catalytic science owing to the high C–H bond dissociation energy (104.9 kcal/mol), low polarizability, and negligible electron affinity of methane.

Methane monooxygenases (MMOs) are enzymes that convert methane into methanol under physiological conditions.[3–5] Since the discovery that MMOs utilize iron or copper oxo species as catalytic centers (Figure 1a), many have explored the synthesis of artificial metal complexes by mimicking their reactive centers. Such studies have greatly succeeded in identifying reactive intermediates and unveiling the reaction mechanism.[5–7] Furthermore, recent studies have clarified that a proton-coupled electron transfer (PCET) pathway renders methane oxidation energetically easier.[8–10] In principle, two important factors should be considered for achieving efficient PCET: (i) positive redox potential for facilitating the electron transfer from methane and (ii) higher oxo-basicity to abstract a H atom from CH_4.[11–13] Despite these insights, the methane oxidation activities of artificial biomimetic molecular catalysts are less than a few tenth of those of the natural enzymes, and moreover, most of the artificial systems can hardly activate the C–H bond of methane. Considering the high reactivity of the MMOs, it should be possible to improve the activities of artificial molecular catalysts by adopting innovative strategies. In general, natural enzymes control the reactivity of their catalytic centers using the coordinating ligands with the aid of higher-order protein structures. However, the preparation of artificial systems that mimic such structures is likely to be tedious and limiting. Therefore, it is necessary to develop a facile methodology to dramatically enhance the activity of molecular iron-oxo species in oxidation reactions.

Here, we demonstrate that close-stacking a μ-nitrido-bridged iron phthalocyanine dimer **1** (Figure 1b) with a double-decker structure onto the surface of graphite is an effective strategy for realizing a catalyst with high methane oxidation activity, rivaling those of natural MMOs. μ-Nitrido-bridged iron porphyrinoid dimers, including a μ-nitrido-bridged iron phthalocyaine dimer, are known to be the most promising class of molecular catalysts based on high-valent iron oxo species for methane oxidation.[14–20] Further, peripheral electron-donating substituents can be introduced into such dimers to improve the catalytic oxidation activity by several folds.[17,20] However, the probability of achieving high oxo-basicity as well as positive potential solely through the introduction of substituents is not high because they are generally in a trade-off relationship with each other. Our recent study on a supramolecular conjugate based on a μ-nitrido-bridged iron porphyrinoid dimer suggested that the extension of the π-stacked structure by including an additional porphyrin into the stack is a feasible approach for enhancing its alkane oxidation activity,[18,19] although the degree of enhancement achieved was not satisfactory. In this context, we surmised that the stacked conjugate of a high-valent iron oxo species of a μ-nitrido-bridged iron phthalocyanine dimer with no bulky peripheral substituents on graphite (**1_{oxo}**/G, Figure 1b) could result in higher methane oxidation activity owing to strong electronic perturbation induced by the effective close-stacking of the units. A single graphene-confined iron ion is known to be effective for methane conversion at ambient temperature.[21] In the case of more facile oxidation reactions such as phenol oxidation, it has been reported that the adsorption of a catalyst with molecular

π-planarity such as iron porphyrin onto the surface of graphene can result in enhanced catalytic activity, although the detailed mechanism of the activation is still unclear.[22] In this study, we also clarify the underlying reasons for the high methane oxidation activity of our graphite-supported double-decker catalyst based on electrochemical measurements combined with surface spectroscopic techniques and computational study.

Results and Discussion

Preparation and characterization of the graphite-supported catalyst.

Although **1** is poorly soluble in many organic solvents in its neutral form, we found that treating graphite with its $1e^-$-oxidized monocationic complex, $\mathbf{1}^+\cdot I^-$ results in the formation of the desired catalyst, **1**/G, in which the neutral form **1** is adsorbed on the graphite surface (Figure 1b). Pyridine is a good solvent for $\mathbf{1}^+\cdot I^-$ because the axial coordination of pyridine with the Fe center of $\mathbf{1}^+\cdot I^-$ prevents its aggregation.[23,24] Heating a mixture of $\mathbf{1}^+\cdot I^-$ and graphite in pyridine at 80 °C was necessary for the efficient adsorption of **1** onto graphite, which was confirmed by the decolorization of the resulting supernatant.

To characterize the structure of the catalyst on the graphite surface, we performed X-ray photoelectron spectroscopy (XPS) and near edge X-ray absorption fine structure (NEXAFS) analyses using highly oriented pyrolytic graphite (HOPG) treated with $\mathbf{1}^+\cdot I^-$ (**1**/HOPG). As shown in Figure S1 (Supplementary Information), after adsorption, the XPS signals corresponding to the iron species in the catalyst shifted slightly to a binding energy that is almost the same as that of **1** (the neutral form), while the peaks corresponding to iodine disappeared completely (Figures S1–S4). This result suggests that $\mathbf{1}^+\cdot I^-$ was reduced by one electron to form the neutral complex, i.e., **1**, after adsorption on graphite. The actual catalyst **1**/G (Figures S5 and S6) showed the same spectral characteristics. Moreover, the angle-dependent N K-edge NEXAFS spectra revealed that **1** was aligned parallel to the graphite surface along its phthalocyanine moiety, indicating π-π stacking interaction between 1 and graphite (Figure 1c).

Heterogeneous oxidation of methane and ethane.

The heterogeneous oxidation of methane or ethane was performed in H_2O (3.0 mL) using the solid-supported catalyst, **1**/G (with 19 μM of **1**), H_2O_2 (189 mM), and TFA (51 mM) under 1.0 MPa gas pressure at 60 °C, and the resulting products were analyzed by GC-MS. Significant amounts of the oxidized products were detected in GC-MS, as shown in Figure 2a and Supplementary Figure S7 and Tables S1 and S2, which indicated that methane or ethane was oxidized in a stepwise manner, as illustrated in Figure 2b. The oxidized products were further characterized by ^{1}H-NMR spectroscopy (Figures S8 and S9). In contrast, the reactions conducted in the absence of methane (or ethane) hardly yielded any of these oxidized products (entries 11 in Tables S1 and S2). As graphite is inherently incapable of oxidizing light alkanes such as methane or ethane under these reaction conditions (entry 16 in Table S1), the obtained results clearly imply that the catalyst adsorbed on graphite catalyzed the oxidation of the two alkanes. Moreover, as the reaction could not be quenched with Na_2SO_3 (entry 12 in Table S2), a radical scavenger, the possibility of a Fenton-type reaction is excluded.[25,20,26] Therefore, the actual reactive species should be a high-valent iron-oxo species that is generated *in situ*.

Next, we calculated the effective total turnover number (TTN_{eff}) as an indicator of the catalytic methane and ethane oxidation activities of the catalyst. TTN_{eff} is defined by Equations (i) and (ii) (or (iii)) shown in Figure 2c. In addition, the effective methane conversion number (MCN_{eff}) is defined by Equations (iv) and (v) to compare the catalytic activity of **1**/G with those of natural MMOs and certain other metal-oxo-based molecular catalysts. The MCN_{eff} indicates the number of methane molecules a single catalyst molecule

can transform, whereas the TTN_{eff} reflects the total number of catalytic oxidation reactions involved.

As shown in Figure 2d, the TTN_{eff}s initially increased almost linearly (up to 4 h) in both the methane and ethane oxidation reactions, suggesting that the reaction center of **1** retained its catalytic activity under the experimental conditions employed in this work. The excellent stability of **1**/G was confirmed by the fact that the TTN_{eff} in the oxidation of ethanol (3.0 M) reached 30,000 only after 1 h of reaction under the same reaction conditions (entry 13 in Table S2). The gradual decrease in the reaction rate after 4 h can be partially attributed to the decomposition of HCOOH, because **1**/G could oxidize HCOOH, as confirmed independently (Figure S10).

As both $\mathbf{1}^+$ consisting of two Fe(IV) ions and its $1e^-$-reduced species (**1**) containing one Fe(III) ion and one Fe(IV) ion are known to be oxidants,[14-17,20] we prepared two different silica-supported catalysts, $\mathbf{1}^+\cdot I^-/SiO_2$ and $\mathbf{1}/SiO_2$, as reference samples. We found that the initial turnover frequency (TTN_{eff}/h) of **1**/G in both the methane and ethane oxidation reactions was considerably higher than those of $\mathbf{1}^+\cdot I^-/SiO_2$ and $\mathbf{1}/SiO_2$ (entries 12–15 in Table S1, entries 14–17 in Table S2, and Figure 2e). The oxidized products observed in the absence of methane or ethane were presumably derived from the organic solvents adsorbed on the solid supports. These results indicate that the significant increase in the oxidizing ability of **1** originates from the interaction between the μ-nitrido-bridged iron phthalocyanine dimer and graphite. The difference in the TTN_{eff}s in the methane and ethane oxidation is apparently due to the difference in the C–H dissociation energies of the two alkanes (104.9 kcal/mol for methane, 101.4 kcal/mol for ethane). Alkane oxidation by iron porphyrinoid in the presence of H_2O_2 generally competes with the catalase reaction, in which the iron-oxo species, the reactive intermediate generated by the reaction with H_2O_2, oxidizes H_2O_2 to O_2.[27] We found that the catalase reaction facilitated by **1**/G was significantly enhanced in comparison with that catalyzed by $\mathbf{1}^+\cdot I^-/SiO_2$ (Figure S11), and almost half of H_2O_2 (52%) was consumed by this reaction under the same reaction conditions after 8 h. This factor also accounts for the gradual decrease in the reaction rates, as shown in Figure 2d.

Further, we investigated the temperature-dependence of the catalytic methane oxidation activity, and the results are summarized in Figure 3a (entries 1 to 4). **1**/G exhibited methane oxidation activity even at room temperature to yield methanol and formaldehyde as major products; this result indicates its high catalytic activity. Its TTN_{eff} was found to increase with the temperature. In the presence of increased amount of H_2O_2 (945 mM) at 100 °C, the TTN_{eff} and MCN_{eff} reached 600 and 200 h^{-1}, respectively (entry 5 in Figure 3a). Furthermore, a similar high catalytic methane oxidation activity could be realized by irradiating the reaction mixture with a high-pressure Xe lamp equipped with an infrared-blocking mirror module without using any temperature-control apparatus (entry 6 in Figure 3a). As the TTN_{eff} was much lower when the photoirradiation-induced reaction was performed at 20 °C with appropriate temperature control (entry 7 in Figure 3a), the high activity under photoirradiation is mainly attributed to the light-induced heating owing to the photothermal effect of graphite.[28,29] In fact, the temperature of the reaction mixture increased to ~70 °C after 1 h of photoirradiation. The realization of a high catalytic activity without using any temperature-control apparatus is apparently an added advantage of using graphite as a solid support.

Given the high catalytic methane oxidation activity of **1**/G, we compared the initial turnover frequencies (TTN_{eff}/h and MCN_{eff}/h) of **1**/G with those of natural MMOs and other highly active metal-oxo-based molecular catalysts (see Figure 3b).[4,17,30] Both the values indicated that **1**/G exhibits a much higher methane oxidation activity compared to those of other efficient biomimetic catalysts reported so far. Moreover, its activity is almost comparable to those of some natural MMOs.

Structure and electronic state of the catalyst on graphite.

To clarify the reasons for the high catalytic activity of **1**/G, the electronic state of the catalyst on graphite was investigated by cyclic voltammetry using **1** adsorbed to the basal plane of graphite in a pyrolytic graphite electrode. A sufficient amount of the catalyst was adsorbed onto the electrode surface by simply dipping the electrode in a pyridine solution of $\mathbf{1}^{+}\cdot I^{-}$. As shown in Figure 4a, the change in the voltammogram of the catalytic center suggests a dramatic change in the electronic structure of the catalyst after its adsorption onto the electrode surface. The graphite electrodes treated with both **1** and $\mathbf{1}^{+}\cdot I^{-}$ yielded almost identical voltammograms (Figure S12), suggesting that $\mathbf{1}^{+}\cdot I^{-}$ was reduced by one electron to turn into neutral species **1** during its adsorption onto the graphite surface. In particular, a reversible $1e^{-}$-redox wave assignable to Fe(IV)-N=Fe(IV)/Fe(III)-N=Fe(IV) showed a significant positive shift ($\Delta E^{\circ\prime}$ = 0.463 V).[31] We confirmed that the difference in the type of counter anion present in the supporting electrolyte and the coordinating solvent associated with the iron species in **1** did not significantly affect the degree of the positive shift, as shown in Figure S13 and Table S4. Therefore, we inferred that the positive shift of the redox potential implies that the SOMO level of **1** decreased significantly after its adsorption to the support. The absolute electrode potential (E_{abs}) calculated from the redox potentials allowed us to confirm that the SOMO level of adsorbed **1** (4.77 V) was lower than that of graphite (~4.5 eV), as shown in Figure 4b.[32,33]

The positive shift in the $1e^{-}$-oxidation waves in the cyclic voltammogram suggests charge transfer from **1** to graphite because the iron center of **1** became more electron-deficient after adsorption. In fact, for monomeric iron(II) phthalocyanine (**Fe(II)Pc**) on graphene, partial charge transfer from iron(II) phthalocyanine to graphite was predicted by theoretical calculations.[34] Therefore, DFT calculations of the stacked conjugate of graphene and **1** with a coordinating H_2O were conducted using the VASP software. The calculations indicated a slight charge transfer from **1** to the graphene surface, as in the case of **Fe(II)Pc**. Interestingly, most of the transferred charges were distributed between graphene and the adsorbed iron(II) phthalocyanine, whereas the non-adsorbed iron(II) phthalocyanine unit including the coordinated H_2O was almost free from the transferred charge, as depicted in Figure 4c. Moreover, the SOMO of **1** interacted in a bonding manner with the π-orbital of graphene to produce a new orbital with a lower energy, consistent with the lowered SOMO level deduced based on the results of electrochemical measurements (Figure 4d).

To confirm the effect of stacking between **Fe(II)Pc** and graphite on the electrochemical properties, cyclic voltammetry was performed on a pyrolytic graphite electrode with **Fe(II)Pc** adsorbed on the basal plane of graphite. The oxidation potential corresponding to Fe(III)/Fe(II) showed a significant positive shift, as shown in Figure S14, although the oxidation process was found to be irreversible. This indicates the instability of the stacked conjugate of positively charged monomeric iron phthalocyanine on the graphite surface, which is in clear contrast with the reversible redox wave observed for **1** adsorbed on the graphite surface (Figure 4a). We confirmed that the catalytic methane oxidation activity of the monomeric **Fe(II)Pc** adsorbed on graphite (**Fe(II)Pc**/G) was much lower than that of **1**/G (Table S1, entry 17), which suggests the superiority of the double-decker structure of **1**/G. It should also be noted that methane oxidation in the presence of **Fe(II)Pc**/G proceeded via a Fenton-type reaction mechanism because it was significantly quenched in the presence of 100 mM Na_2SO_3 (Table S1, entry 19).

Proposed mechanism for activation of the catalyst.

The reactive species in alkane oxidation catalyzed by a μ-nitrido-bridged iron phthalocyanine dimer is reported to be a high-valent iron-oxo species generated by the

reaction of the catalyst with H_2O_2 (Figure 1a).[14,16] We confirmed the generation of iron-oxo species on the graphite surface by high-resolution MALDI-TOF mass spectroscopy. As shown in Figure S16, short-time treatment of **1**/HOPG with $H_2{}^{16}O_2$ or $H_2{}^{18}O_2$ resulted in the generation of the $[\mathbf{1}+O]^+$ species, which corresponds to the mass number of the high-valent iron-oxo species, $\mathbf{1_{oxo}}$ generated on HOPG.

According to the results obtained, we propose a possible mechanism for the high methane conversion in the presence of **1**/G based on the reaction of $\mathbf{1_{oxo}}$, as illustrated in Figure 4e. The reaction of **1**/G with H_2O_2 results in a H_2O_2 adduct (**1(HOOH)**/G). Heterolytic cleavage of the O–O bond in **1(HOOH)** produces the high-valent iron-oxo species, $\mathbf{1_{oxo}}$/G, which acts as a reactive intermediate for methane oxidation. Based on the knowledge of the PCET mechanism, key factors to be considered for achieving efficient methane oxidation are high oxo-basicity for efficient H atom abstraction and a more positive redox potential of the catalyst for achieving electron transfer from methane.[8–13] As the electronic structure of $\mathbf{1_{oxo}}$ is similar to that of **1**, in which a SOMO with S = 1/2 spin is distributed mainly over the Fe–N=Fe center,[14,35] it can be assumed that the SOMO level of $\mathbf{1_{oxo}}$ was stabilized in a manner similar to that observed for **1** (Figure 4f). This is likely to be beneficial for achieving a more positive redox potential of $\mathbf{1_{oxo}}$. On the other hand, partial charge transfer from the catalyst to graphite seems to be unfavorable for both the electron donation from the iron phthalocyanine of **1(HOOH)**/G to facilitate the heterolytic cleavage of O–O bonds and the high oxo-basicity of $\mathbf{1_{oxo}}$. In fact, in the case of monomeric iron tetraphenyl porphyrin, it is known that electron-withdrawing substituents introduced on the *meso*-phenyl groups decrease the formation rate of the high-valent iron oxo species.[36] However, in the case of **1**/G, owing to the double-decker structure, positive charges could localize only on the phthalocyanine unit directly stacked on graphite, as shown in Figure 4c, and did not significantly affect the oxo-basicity and formation rate of the oxo species. Overall, **1**/G showed high catalytic activity in methane oxidation.

Conclusion

We demonstrated a graphite-supported molecular catalyst that exhibits high activity in methane oxidation, comparable to that of MMOs. This catalyst consists of a μ-nitrido-bridged iron phthalocyanine dimer with a double-decker structure closely stacked on a graphite support. The catalytic oxidation activity of the μ-nitrido-bridged iron phthalocyanine dimer increased dramatically after its adsorption on the graphite surface. In addition, the photoirradiation of the catalyst led to high catalytic methane oxidation activity without requiring any temperature control apparatus owing to the photothermal effect of the graphite support. On the other hand, monomeric iron(II) phthalocyanine adsorbed on the graphite surface exhibited much lower catalytic activity than that of the double-decker complex.

Spectroscopic and electrochemical analyses of the catalyst suggested that a lower SOMO level of the high-valent iron-oxo species, which is beneficial for PCET with methane, could be achieved by stacking the catalyst on graphite. We suggest that the double-decker structure of the catalyst could have contributed to the prevention of the decrease in the formation rate of the reactive iron-oxo species as well as the decrease in the oxo-basicity. Furthermore, the double-decker structure ensures the stability of the catalytic center during oxidation. This graphite-supported double-decker-type complex may also be used to fabricate electrodes. The exploitation of the interaction of the solid support with the double-decker complex could prove to be a unique strategy for overcoming the limitations of solid-supported molecular catalysts not only in methane oxidation, but also in a wide variety of other reactions.

Experimental Procedures
Resource availability

Lead contact
Further information and requests for additional details should be directed to and will be fulfilled by the Lead Contact, Yasuyuki Yamada (yamada.yasuyuki@h.mbox.nagoya-u.ac.jp).

Materials availability
All materials generated in this study are available from the lead contact without restriction.

Data and code availability
The published article includes all datasets generated or analyzed during this study.

Supplemental information
Supplemental Information (Supplemental experimental procedures, Figures S1–S16, and Tables S1–S4) can be found online at XXXX.

Acknowledgments
We thank Prof. J. Yoshinobu and Prof. K. Asakura for the fruitful discussion with them. This work was financially supported by JST PRESTO (Number 14J04135), a JSPS KAKENHI Grant-in-Aid for challenging Exploratory Research (Number 16K13961), and a Grant-in-Aid for Scientific Research (B) (Number 19H02787) awarded to YY, a JSPS KAKENHI Grant-in-Aid for Scientific Research (A) (15H02167 and 19H00902) awarded to KeT, and JST CREST "Innovative Catalysts" JPMJCR15P5 awarded to KY. This study was also supported by the Cooperative Research Program of Institute for Catalysis, Hokkaido University. (Proposal 18B1013). The computations in this work were primarily performed using the computer facilities at Research Institute for Information Technology, Kyushu University.

References
1. Ravi, M., Ranocchiari, M., van Bokhoven, J. A. (2017). The direct catalytic oxidation of methane to methanol–a critical assessment. Angew. Chem. Int. Ed. *56*, 16464–16483.
2. Schwach, P., Pan, X., Bao, X. (2017). Direct conversion of methane to value-added chemicals over heterogeneous catalysts: challenges and prospect. Chem. Rev. *117*, 8497–8520.
3. Tinberg, C. E., Lippard, S. J. (2011). Dioxygen Activation in Soluble Methane Monooxygenase. Acc. Chem. Res. *44*, 280–288.
4. Sirajuddin, S., Rosenzweig, A. C. (2015). Enzymatic Oxidation of Methane. Biochemistry *54*, 2283–2294.
5. Wang, V. C.-C., Maji, S., Chen, P. P.-Y., Lee, H. K., Yu, S. S.-F., Chan, S. I. (2017). Alkane Oxidation: Methane Monooxygenases, Related Enzymes, and Their Biomimetics. Chem. Rev. *117*, 8574–8621.
6. McDonald, A. R., Que Jr, L. (2013) High-valent nonheme iron-oxo complexes: Synthesis, structure, and spectroscopy. Coord. Chem. Rev. *257*, 414–428.
7. Guo, M., Corona, T., Ray, K., Nam W. (2019). Heme and Nonheme High-Valent Iron and Manganese Oxo Cores in Biological and Abiological Oxidation Reactions. ACS Cent. Sci. *5*, 13–28.

8. Weinberg, D. R., Gagliardi, C. J., Hull, J. F., Murphy, C. F., Kent, C. A., Westlake, B. C., Paul, A., Ess, D. H., McCafferty, D. G., Meyer, T. J. (2012). Proton-coupled electron transfer. Chem. Rev. *112*, 4016–4093.
9. Hammes-Schiffer, S. (2015). Proton-Coupled Electron Transfer: Moving Together and Charging Forward. J. Am. Chem. Soc. *137*, 8860–8871.
10. Klein, J. E. M. N., Knizia, G. (2018). cPCET versus HAT: A Direct Theoretical Method for Distinguishing X–H Bond-Activation Mechanism. Angew. Chem. Int. Ed. *57*, 11913–11917.
11. Fujii, H. (1993). Effects of the Electron-Withdrawing Power of Substituents on the Electronic Structure and Reactivity in Oxoiron(IV) Porphyrin π-Radical Complex. J. Am. Chem. Soc. *115*, 4641–4648.
12. Comba, P., Löhr, A.-M., Pfaff, F., Ray. K. (2020). Redox Potential of High-Valent Iron-, Cobalt-, and Nickel-Oxido Complexes: Evidence for Exchanging Enhanced Reactivity. Isr. J. Chem. *60*, 957–962.
13. Green, M. T., Dawson, J. H., Gray, H. B. (2004). Oxoiron(IV) in Chloroperoxidase Compound II Is Basic: Implications for P450 Chemistry. Science *304*, 1653–1656.
14. Afanasiev, P., Sorokin, A. B. (2016). μ–Nitrido diiron macrocyclic platform: particular structure for particular catalysis. Acc. Chem. Res. *49*, 583–593.
15. Sorokin, A. B., Kudrik, E. V., Bouchu, D. (2008). Bio-inspired oxidation of methane in water catalyzed by *N*-bridged diiron phthalocyanine complex. Chem. Commun. 2562–2564.
16. Kudrik, E. V., Afanasiev, P., Alvarez, L. X., Dubourdeaux, P., Clémancey, M., Latour, J.-M., Blondin, G., Bouchu, D., Albrieux, F., Nefedov, S. E., Sorokin, A. B. (2012). An *N*-bridged high-valent diiron-oxo species on a porphyrin platform that can oxidize methane. Nature Chem. *4*, 1024–1029.
17. ˙Is¸ci, Ü., Faponle, A. S., Afanasiev, P., Albrieux, F., Briois, V., Ahsen, V., Dumoulin, F., Sorokin, A. B., de Visser, S. P. (2015). Site-selective formation of an iron(iv)-oxo species at the more electron-rich iron atom of heteroleptic μ–nitrido diiron phthalocyanines. Chem. Sci. *6*, 5063–5075.
18. Yamada, Y., Morita, K., Mihara, N., Igawa, K., Tomooka, K., Tanaka, K. (2019). Catalytic methane oxidation by a supramolecular conjugate based on a μ-nitrido-bridged iron porphyrinoid dimer. New J. Chem. *43*, 11477–11482.
19. Mihara, N., Yamada, Y., Takaya, H., Kitagawa, Y., Igawa, K., Tomooka, K., Fujii, H., Tanaka, K. (2019). Site-selective supramolecular complexation activates catalytic ethane oxidation by a nitride-bridged iron porphyrinoid dimer. Chem. Eur. J. *25*, 3369–3375.
20. Yamada, Y., Kura, J., Toyoda, Y., Tanaka, K. (2021). High Catalytic Methane Oxidation Activity of Monocationic μ-Nitrido-Bridged Iron Phthalocyanine Dimer with Sixteen Methyl Groups. Dalton Trans. *50*, 6718–6724.
21. Cui, X., Li, H., Wang, Y., Hu, Y., Hua, L., Li, H., Han, X., Liu, Q., Yang, F., He, L., Chen, X., Li, Q., Xiao, J., Deng, D., Bao, X. (2018). Room-temperature methane conversion by graphene-confined single iron atoms. Chem *4*, 1902–1910.
22. Xue, T., Jiang, S., Qu, Y., Su, Q., Cheng, R., Dubin, S., Chiu, C.-Y., Kaner, R., Huang, Y., Duan, X. (2012) Graphene-Supported Hemin as a Highly Active Biomimetic Oxidation Catalyst. Angew. Chem. Int. Ed. *51*, 3822–3825.
23. Yamada, Y., Sugiura, T., Morita, K., Ariga-Miwa, H., Tanaka, K. (2019). Improved synthesis of monocationic μ-nitrido-bridged iron phthalocyanine dimer with no peripheral substituents. Inorg. Chim. Acta. *489*, 160-163.
24. Ercolani, C., Gardini, M., Pennesi, G., Rossi, G., Russo, U. (1988). High-valent iron phthalocyanine μ-nitrido dimers. Inorg. Chem. *27*, 422-424.
25. Hammond, C., Forde, M. M., Ab Rahim, M. H., Thetford, A., He, Q., Jenkins, R. L.,

Dimitratos, N., Lopez-Sanchez, J. A., Dummer, N. F., Murphy, D. M., Carley, A. F., Taylor, S. H., Willock, D. J., Stangland, E. E., Kang, J., Hagen, H., Kiely, C. J., Hutchings, G. J. (2012). Direct catalytic conversion of methane to methanol in an aqueous medium by using copper-promoted Fe-ZSM-5. Angew. Chem. Int. Ed. *51*, 5129–5133.

26. Yamada. Y., Kura, J., Toyoda, Y., Tanaka, K. (2020). μ-Nitrido-bridged iron phthalocyanine dimer bearing eight peripheral 12-crown-4 units and its methane oxidation activity. New J. Chem. *44*, 19179–19183.
27. Ghosh, A., Mitchell, D. A., Chanda, A., Ryabov, A. D., Popescu, D. L., Upham, E. C., Collins, G. J., Collins, T. J. (2008). Catalase-peroxide activity of iron(III)-TAML activators of hydrogen peroxide. J. Am. Chem. Soc. *130*, 15116–15126.
28. Han, B., Zhang, Y.-L., Chen, Q.-D. Sun, H.-B. (2018) Carbon-Based Photothermal Actuators. Adv. Funct. Mater. *28*, 1802235.
29. Liu, J., Cui, L., Losic, D. (2013) Graphene and graphite oxide as new nanocarriers for drug delivery applications. Acta Biomaterialia *9*, 9243–9257.
30. Nagababu, P., Yu, S. S.-F., Maji, S., Ramu, R., Chan, S. I. (2014). Developing an efficient catalyst for controlled oxidation of small alkanes under ambient conditions. Catal. Sci. Technol. *4*, 930-935.
31. Bottomley, L. A., Gorce, J.-N., Goedken, V. L., Ercolani, C. (1985). Spectroelectrochemistry of a μ-nitrido-bridged iron phthalocyanine dimer. Inorg. Chem. *24*, 3733–3737.
32. Trassatti, S. (1986). The absolute electrode potential: an explanatory note. Pure & Appl. Chem. *58*, 955–966.
33. Akada, K., Obata, S., Saiki, K. (2019) Work Function Lowering of Graphite by Sequential Surface Modifications: Nitrogen and Hydrogen Plasma Treatment. ACS Omega *4*, 16531–16535.
34. Feng, S., Luo, N., Tang, A., Chen, W., Zhang, Y., Huang, S., Dou, W. (2019). Phthalocyanine and metal phthalocyanines adsorbed on graphene: A density functional study. J. Phys. Chem. C. *123*, 16614–16620.
35. Colomban, C., Kudrik, E. V., Briois, V., Shwarbrick, J. C., Sorokin, A. B., Afanasiev, P. (2014). X-ray absorption and emission spectroscopies of X-bridged diiron phthalocyanine complexes $(FePc)_2X$ (X = C, N, O) combined with DFT study of $(FePc)_2X$ and their high-valent diiron oxo complexes. Inorg. Chem. *53*, 11517–11530.
36. Yamaguchi, K., Watanabe, Y., Morishima, I. (1992). Push Effect on the Heterolytic O–O Bond Cleavage of Peroxoiron(III) Porphyrin Adducts.

Author contributions

Y.Y conceived the project, designed and performed the experiments, and analyzed the data. K.M., T.S., N.M, and Y.T. synthesized the catalysts and performed the gas reactions. T.K. performed MALDI-TOF MS analysis of the reactive intermediate. M.N. and H.T. performed NEXAFS measurements and analysis. Y. T. and K. Y. performed DFT calculation. H.A-.M., S.T., and T.K. performed XPS measurements and analysis. Y.Y., N.N., Ki.T., Y.H., and K.A. elucidated the activation mechanism. Y.Y. and Ke.T. cowrote the manuscript. All authors discussed the results and commented on the manuscript.

Declaration of interest

The authors declare no competing interests.

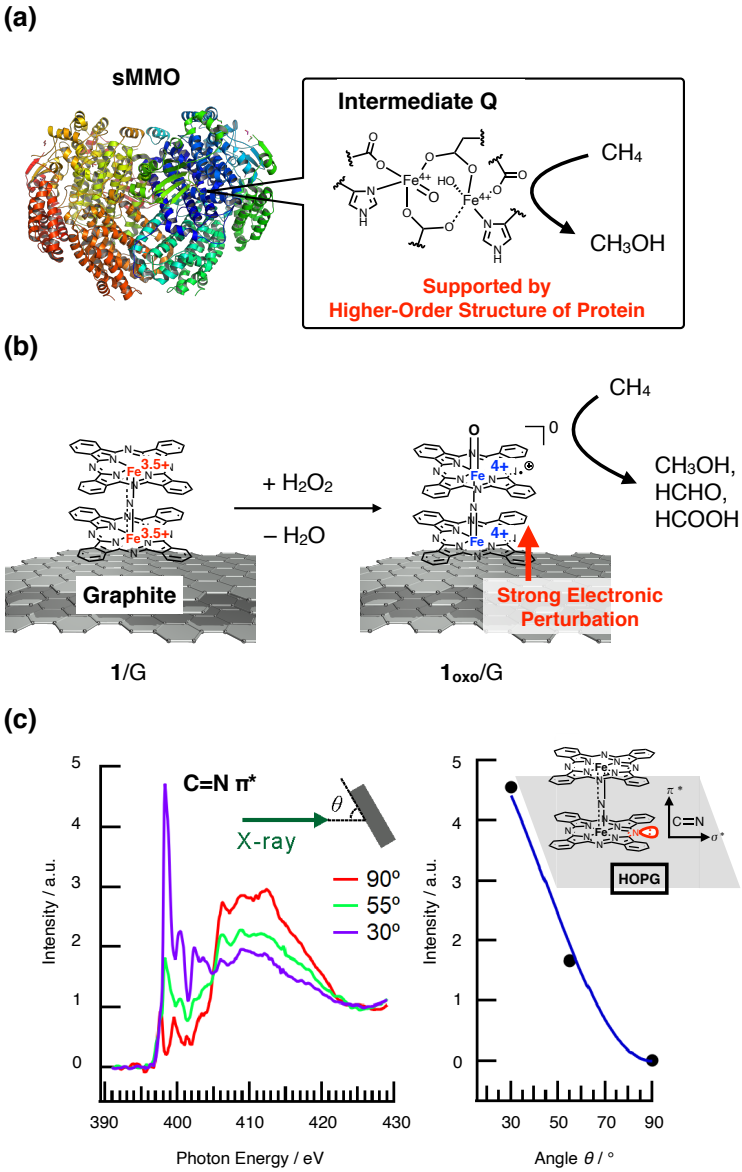

Figure 1. Design and characterization of a graphite-supported μ-nitrido-bridged iron phthalocyanine dimer (1/G) as an efficient methane oxidation catalyst. a, High-valent iron-oxo species in a soluble methane monooxygenase (sMMO). **b,** Generation of a high-valent iron-oxo species of a graphite-supported μ-nitrido-bridged iron phthalocyanine dimer **1**/G (**1**$_{oxo}$/G) for methane oxidation. **c,** Angle-dependent N K-edge NEXAFS spectra of a HOPG substrate adsorbed with the μ-nitrido-bridged iron phthalocyanine dimer (**1**/HOPG). Detailed analysis of the NEXAFS results is given in the Supplementary Information (page S13).

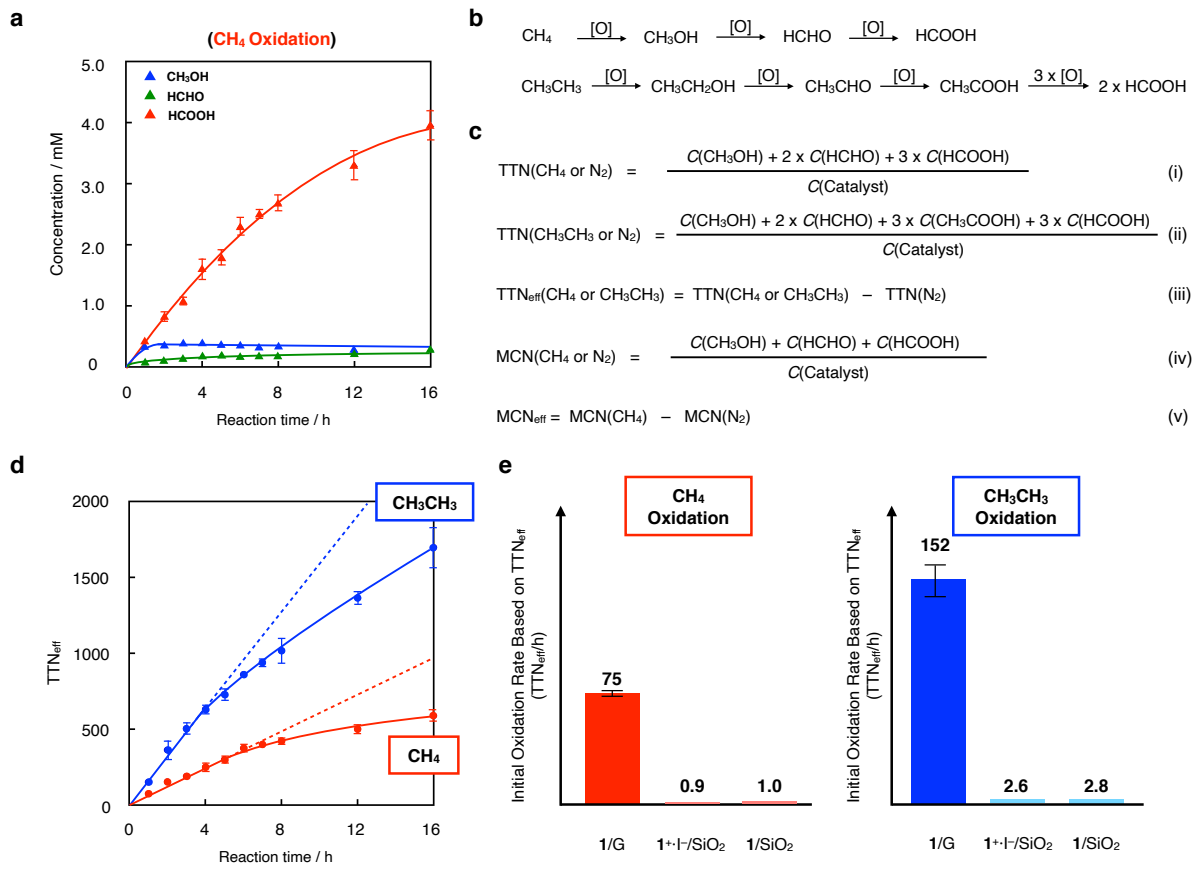

Figure 2. Catalytic activities of the graphite-supported μ-nitrido-bridged iron phthalocyanine dimer (1/G) in the oxidation of methane and ethane. a, Time-dependent change in the concentration of each oxidized product during the oxidation of methane (1.0 MPa) under the catalysis of **1**/G (19 μM as **1**) in an aqueous solution (3.0 mL) containing H_2O_2 (189 mM) and TFA (51 mM) at 60 °C. **b,** Stepwise oxidation reactions of methane and ethane. **c,** Definitions of the effective total turnover number (TTN_{eff}) of the catalyst in methane and ethane oxidation, and effective methane oxidation number (MCN_{eff}). **d,** Time-dependent variation in the TTN_{eff} of **1**/G in methane and ethane oxidation. **e,** Comparison of the TTN_{eff} of **1**/G in methane and ethane oxidation with those of reference samples ($\mathbf{1}^{+}\cdot I^{-}$ and its $1e^{-}$-reduced species, **1** loaded on silica supports). Error bars in **a**, **d**, and **e** indicate the S.D. of three independent reactions conducted using different batches of **1**/G.

(a)

Entry	Catalyst	Reaction Time / h	Reaction Temperature / °C	H_2O_2 / mM	Additional Conditions	[CH_3OH] / mM	[HCHO] / mM	[HCOOH] / mM	TTN(CH_4) or TTN(N_2)	TTN_{eff}	MCN(CH_4) or MCN(N_2)	MCN_{eff}
1	**1**/G	8	25	189	•••	0.32	0.29	0	47	22	32	13
2	**1**/G	8	40	189	•••	0.29	0.39	0.57	145	118	65	44
3	**1**/G	1	80	189	•••	0.27	0.31	0.81	186	140	78	57
4	**1**/G	1	100	189	•••	0.38	0.89	2.80	591	549	228	208
5	**1**/G	1	100	945	•••	0.28	0.40	3.81	702	630	252	218
6	**1**/G	1	No temp. control	189	Photo-irradiation	0.32	1.08	2.55	567	496	221	189
7	**1**/G	1	20	189	Photo-irradiation	0.13	0.22	0.23	72	3	33	1

(b)

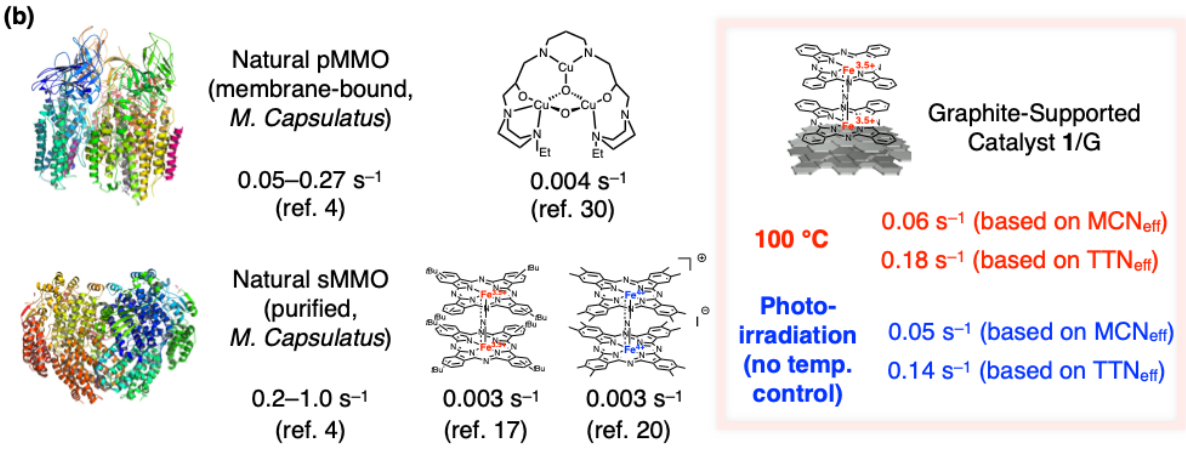

Figure 3. Comparison of catalytic methane oxidation activities of natural and artificial metal-oxo-based molecular catalysts. a, Summary of the results of methane oxidation. Reactions were performed under 1.0 MPa CH_4 pressure using a graphite-supported catalyst (**1**/G or **Fe(II)Pc**/G containing 19 μM of the catalyst) in an aqueous solution (3.0 mL) containing H_2O_2 (189 mM or 945 mM) and TFA (51 mM) at the given temperature or the reaction conditions. The results of the reactions in the absence of CH_4 (under N_2; 1.0 MPa) are summarized in Table S3 in the Supplementary Information. The details of the reaction conducted under photoirradiation are provided in the Supplementary Information. **b,** Comparison of the turnover frequencies of MMOs and certain artificial metal-oxo-based molecular catalysts. The turnover frequencies of efficient molecular catalysts reported to date (Refs. 17, 20, and 30) were calculated based on their total turnover numbers. The turnover frequencies of **1**/G calculated based on both the effective total turnover number (TTN_{eff}) and the effective methane oxidation number (MCN_{eff}) are shown.

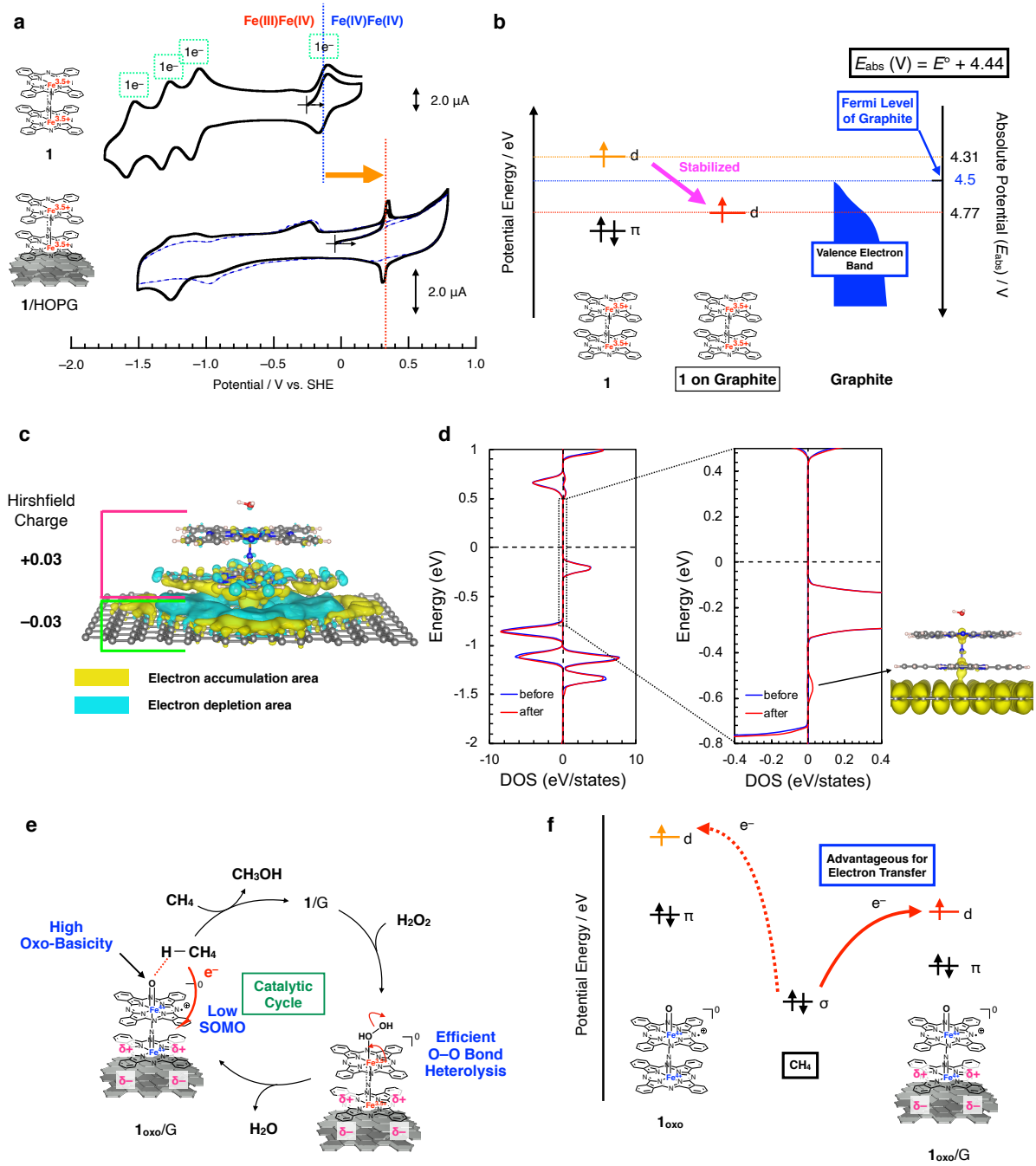

Figure 4. Elucidation of the roles of the graphite support and double-decker structure of the μ-nitrido-bridged iron phthalocyanine dimer in the high methane oxidation activity of 1/G. a, Comparison of the cyclic voltammograms of **1** in a 400 μM solution (top) and the μ-nitrido-bridged iron phthalocyanine dimer adsorbed on the graphite basal plane in a pyrolytic graphite electrode (bottom, black line). The blue dashed line in the bottom voltammograms represents the results obtained with a bare pyrolytic graphite electrode (without **1**). All voltammograms were recorded in a pyridine solution containing 100 mM $^{n}Bu_4N^{+}PF_6^{-}$ ($TBAPF_6$) at 20 °C at the scan rate of 0.1 V/s. **b,** Comparison of the SOMO energy levels for the μ-nitrido-bridged iron phthalocyanine dimer, **1** (neutral species, in a pyridine solution), and for **1** adsorbed on the graphite surface (**1**/HOPG) with the Fermi level of graphite obtained based on the absolute redox potentials calculated from the cyclic

voltammograms. **c**, Charge density difference for the adsorption of **1** on the surface of graphene. Electron accumulation and depletion are represented by yellow and blue areas, respectively (isovalue is set to 5.0×10^{-4} Å^{-3}). **d**, Comparison of spin-up (positive values) and spin-down (negative values) density of states (DOS) projected on the Fe atom closer to G before (blue) and after (red) adsorption. The Fermi level is set to 0 eV. A close-up view of the Fermi level is also shown. A new state is generated at $E = -0.58$ eV upon adsorption. The charge density isosurface corresponding to the state is shown in the inset (isovalue is set to 3.0×10^{-4} Å^{-3}). **e**, Proposed reactions involved in the high methane conversion under the catalysis of **1**/G based on the reaction of $\mathbf{1_{oxo}}$. **f**, A lower SOMO level of the high-valent iron-oxo species of the μ-nitrido-bridged iron phthalocyanine dimer could be achieved through its interaction with graphite. This is likely to favor the proton-coupled electron transfer from methane.